

Artificial Multiferroics and Enhanced Magnetoelectric Effect in van der Waals Heterostructures

Yan Lu,^{1,2} Ruixiang Fei,¹ Xiaobo Lu,¹ Linghan Zhu,¹ Li Wang,^{2} and Li Yang^{1*}*

¹Department of Physics and Institute of Materials Science and Engineering,
Washington University, St. Louis, MO 63130, USA

²Department of Physics, Nanchang University, Nanchang 330031, China

Keywords: 2D multiferroics, magnetoelectric effect, van der Waals heterostructure,
first-principles calculation, CrI₃

Abstract: Multiferroic materials with coupled ferroelectric and ferromagnetic properties are important for multifunctional devices due to their potential ability of controlling magnetism via electric field, and vice versa. The recent discoveries of two-dimensional ferromagnetic and ferroelectric materials have ignited tremendous research interest and aroused hope to search for two-dimensional multiferroics. However, intrinsic two-dimensional multiferroic materials and, particularly, those with strong magnetoelectric couplings are still rare to date. In this paper, using first-principles simulations, we propose artificial two-dimensional multiferroics via a van der Waals heterostructure formed by ferromagnetic bilayer chromium triiodide (CrI₃) and ferroelectric monolayer Sc₂CO₂. In addition to the coexistence of ferromagnetism and ferroelectricity, our calculations show that, by switching the electric polarization of Sc₂CO₂, we can tune the interlayer magnetic couplings of bilayer CrI₃ between ferromagnetic and antiferromagnetic states. We further reveal that such a strong

magnetoelectric effect is from a dramatic change of the band alignment induced by the strong build-in electric polarization in Sc_2CO_2 and the subsequent change of the interlayer magnetic coupling of bilayer CrI_3 . These artificial multiferroics and enhanced magnetoelectric effect give rise to realizing multifunctional nanoelectronics by van der Waals heterostructures.

1. INTRODUCTION

Coupled ferroelectricity and ferromagnetism, *i.e.*, the magnetoelectric effect, play critical roles for applications of multifunctional devices due to its unique ability of tuning magnetism by applying electric field, and vice versa.^{1,2} However, multiferroic materials with the strong magnetoelectric effect are still scarce due to a few well-known challenges. First, ferroelectricity is usually from the *s* and *p* electrons and requires materials with empty or fully occupied *d* orbitals. However, ferromagnetism is usually from *d* electrons and requires those with partially occupied *d* orbitals.³ Second, the coupling between ferroelectricity and ferromagnetism is usually weak for multiferroic materials, in which ferroelectricity and ferromagnetism come from two types of *d*-orbital elements.

Recent advances in realizing ferroics in two-dimensional (2D) materials may give hope to overcoming these fundamental challenges of traditional bulk materials. For example, novel 2D materials, such as group-IV monochalcogenides,⁴⁻⁸ group-V monolayer,⁹ III-VI₃ van der Waals (vdW) materials,¹⁰⁻¹⁴ transition metal thiophosphate (TMTP)

family,^{15–18} and oxygen-functionalized scandium carbide MXene (Sc_2CO_2),¹⁹ are reported to be ferroelectric (FE) materials because their vdW interfaces can avoid the known depolarization effect of bulk structures.^{20–22} Meanwhile, 2D ferromagnetism has been recently achieved in vdW materials, such as few-layer $\text{Cr}_2\text{Ge}_2\text{Te}_3$,²³ CrI_3 ,²⁴ and Fe_3GeTe_2 ,^{25,26} spurring substantial interests to fabricate ultra-thin magnetic devices and study fundamental properties, such as magnons, spin liquids, and many other quantum states in reduced-dimensional structures.^{27–44} All these advances pave the way for exploring the existence of 2D multiferroics and magnetoelectronic couplings.

To date, there have been predictions of 2D multiferroic materials. Monolayer group-IV monochalcogenides, e.g., SnSe and GeSe , have been predicted to be multiferroic with the coexistence of ferroelasticity and ferroelectricity.^{4,45} Hole-doped α - SnO monolayer has been predicted to be multiferroic with the coexistence of ferromagnetism and ferroelasticity.⁴⁶ Monolayer TMPCs- CuMP_2X_6 ($\text{M}=\text{Cr}, \text{V}; \text{X}=\text{S}, \text{Se}$)⁴⁷ and charged CrBr_3 monolayer⁴⁸ have been predicted to exhibit multiferroicity with the coexistence of ferromagnetism and ferroelectricity. However, these structures do not exhibit strong magnetoelectronic effects because of the intrinsic limit of the weak coupling between different d -orbital elements. Interestingly, a recent work by Zhang' group⁴⁹ predicted that multiferroics can be achieved by artificial vdW heterostructures, and the magnetic easy axis of $\text{Cr}_2\text{Ge}_2\text{Te}_3$ can be tuned by the polarization of the nearby ferroelectric layer. These advance shed light on searching for multiferroics and further turning on/off magnetism in artificial vdW heterostructures.

In this work, using first-principles density functional theory (DFT) simulations, we propose 2D artificial multiferroic realized by a vdW heterostructure via stacking bilayer CrI_3 and monolayer Sc_2CO_2 . Importantly, we show that tuning the polarization direction of the Sc_2CO_2 layer can switch the interlayer magnetic order of bilayer CrI_3 to be ferromagnetic (FM) or antiferromagnetic (AFM), *i.e.*, turning on/off the magnetism. Our analysis indicates that this enhanced coupling between ferroelectricity and magnetic order is from the significant change of interlayer band alignment and subsequent interlayer charge transfers. Therefore, artificial vdW multiferroics may provide ample space to realize strong magnetoelectric couplings for future multifunctional nanoelectronics and devices.

2. RESULTS AND DISCUSSION

The 2D artificial multiferroics is constructed by stacking bilayer CrI_3 with monolayer Sc_2CO_2 to form a vdW 2L- $\text{CrI}_3/\text{Sc}_2\text{CO}_2$ heterostructure. The in-plane lattice constant of free-standing CrI_3 is 6.87 Å, and that of Sc_2CO_2 is 3.37 Å. By using a 2×2 supercell of monolayer Sc_2CO_2 to match bilayer CrI_3 , as shown in Figure 1a, the in-plane lattice mismatch can be reduced to be less than 2%, which is widely accepted in first-principles studies.^{49–51}

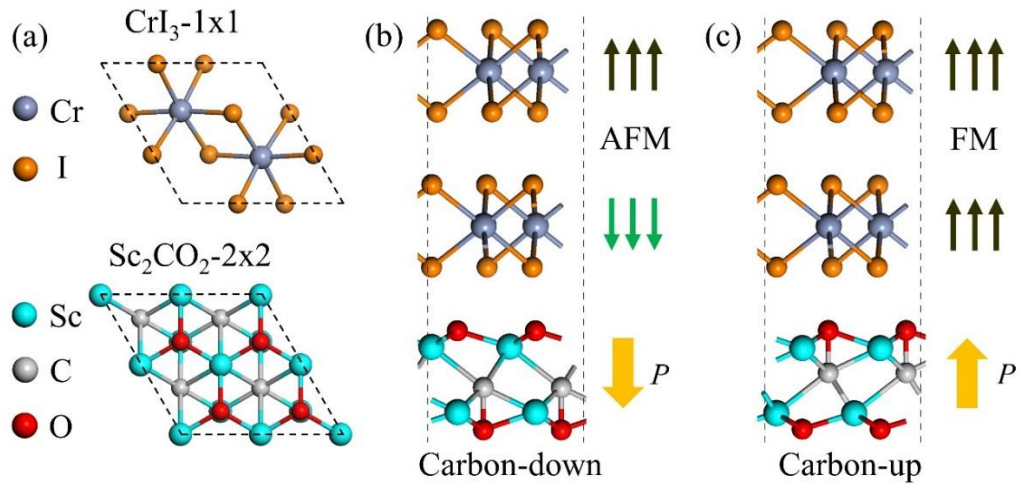


Figure 1. (a) Top-views of 1×1 unit cell of CrI_3 and 2×2 unit cell of Sc_2CO_2 . (b) and (c) Side views of $2\text{L-CrI}_3/\text{Sc}_2\text{CO}_2$ heterostructures with carbon-down and carbon-up configurations of the Sc_2CO_2 layer, respectively. The black and green thin arrows denote the spin directions in 2L-CrI_3 . The golden thick arrow denotes the direction of the out-of-plane electric polarization in Sc_2CO_2 .

Monolayer Sc_2CO_2 is predicted to exhibit both in-plane and out-of-plane electric polarizations.¹⁹ Free-standing monolayer Sc_2CO_2 exhibits an out-of-plane electric polarization of $1.60 \mu\text{C}/\text{cm}^3$, which is reported to be the largest for a monolayer material. This polarization can be switched by the displacement of the C atoms, as denoted by carbon-down and carbon-up configurations shown in Figures 1b and 1c. The calculated energy barrier is 0.52 eV per formula unit between the Carbon-down and Carbon-up configurations for Sc_2CO_2 .¹⁹ The coercive field can be up to 2.5 V/nm if the temperature effect is not taken into account. However, this coercive field can be substantially reduced after condiering finite temperature.

CrI₃ is an intensively studied 2D magnetic material. With the help of out-of-plane magnetic anisotropy,⁵² the 2D structure hold a long-range magnetic order by gapping low-energy modes of magnons. It has two types of interlayer stacking styles: the high-temperature (HT) and low-temperature (LT) phases.²⁷ Importantly, despite the robust intralayer FM order, the interlayer magnetic coupling of few-layer CrI₃ is sensitive to the stacking structure: it is FM for the LT phase but AFM for the HT phase.^{53–56} Surprisingly, most experimental samples exhibit the HT phase with a subsequent layer-dependent magnetism.^{35,57–61} Therefore, we choose the HT-phase of bilayer CrI₃ in our studied heterostructure. More thorough studies reveal that the energy difference between interlayer FM and AFM order is so small (~ 0.1 meV/ Cr ion), explain the highly tunable (by strain, doping, and magnetic field) magnetism observed in the HT-phase CrI₃. This tunable interlayer magnetism also gives hope to realizing magnetoelectric effects in this 2D structure.

After forming the 2L-CrI₃/Sc₂CO₂ heterostructure shown in Figure 1, we find that the FE order of the Sc₂CO₂ layer and the magnetic order of bilayer CrI₃ coexist, indicating the multiferroics. More interestingly, the out-of-plane electric polarization from the neighboring Sc₂CO₂ layer can substantially switch the magnetic order of bilayer CrI₃. As shown in Figure 1b, when the Sc₂CO₂ layer is in the carbon-down configuration with a downward polarization, bilayer CrI₃ keeps the AFM interlayer order, and the AFM state is about 0.37 meV/unit cell lower than the FM state. However, when the Sc₂CO₂ layer switches to the carbon-up configuration with an upward polarization

(Figure 1c), bilayer CrI_3 will be tuned to the FM interlayer order, and the FM state is about 1.41 meV/unit-cell lower than the AFM state. As a result, the overall magnetism can be turned on or off by the electric polarization (or external gate field), resulting in a significant magnetoelectric effect.

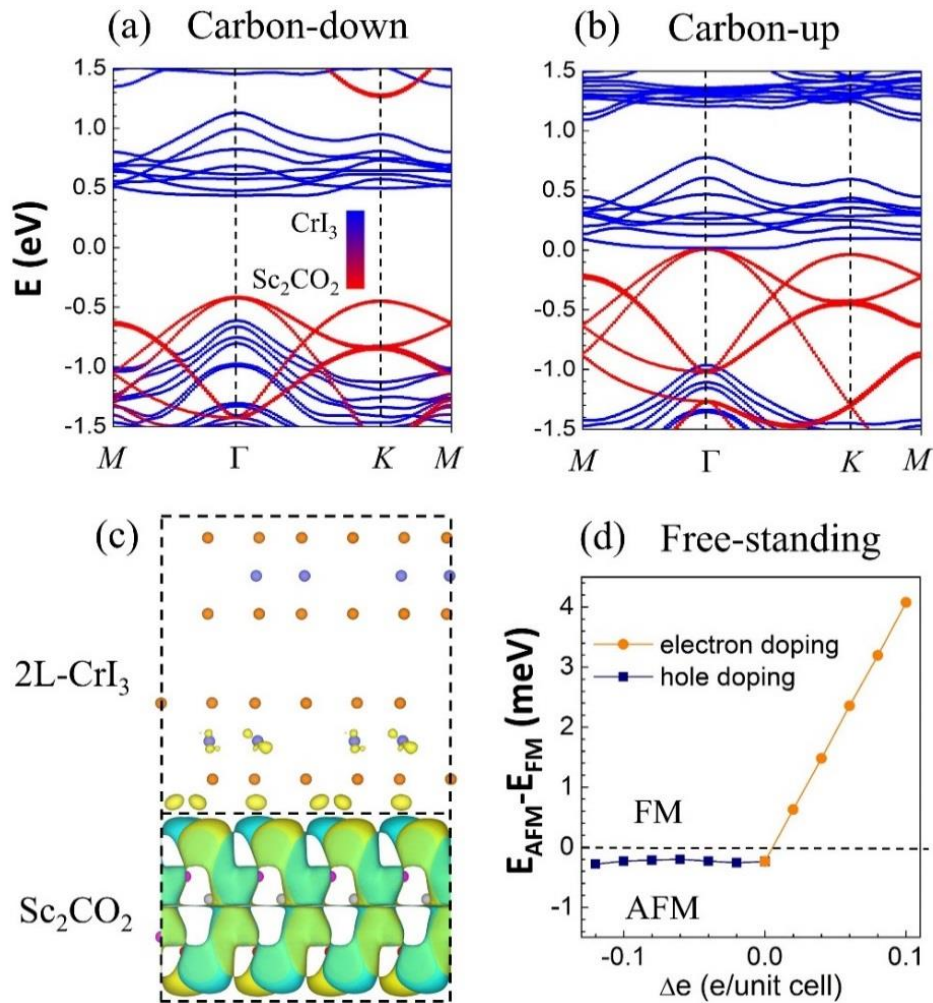


Figure 2. The DFT+U calculated band structure of $2\text{L-CrI}_3/\text{Sc}_2\text{CO}_2$ heterostructures for (a) carbon-down and (b) carbon-up configurations, respectively. Colors indicate the weight of bands from CrI_3 (blue) and Sc_2CO_2 (red). (c) The differential charge distribution of the $2\text{L-CrI}_3/\text{Sc}_2\text{CO}_2$ heterostructure calculated by subtraction of the electron distribution of the carbon-down configuration from that of the carbon-up

configuration. The isosurface value is $0.001 e/\text{Bohr}^3$. The yellow color means electron accumulation, and the cyan color means electron loss. (d) Electron and hole doping effects on the energy difference between AFM and FM interlayer couplings for free-standing bilayer HT CrI₃.

To understand such multiferroic and magnetoelectric coupling, we have plotted the electronic band structures of these 2L-CrI₃/Sc₂CO₂ heterostructures with the electric polarization up and down, respectively. In Figure 2a, for the carbon-down configuration, a finite band gap around 0.85 eV is observed, and the heterostructure forms a type II band alignment, in which the valence band maximum (VBM) comes from the Sc₂CO₂ layer, and the conduction band minimum (CBM) comes from bilayer CrI₃. However, for the carbon-up configuration, the band gap is closed under the polarization field. The CBM from bilayer CrI₃ touches the VBM from the Sc₂CO₂ layer, forming a type-III band alignment, as shown in Figure 2b.

Our further analysis shows that such a band crossing will introduce a charge transfer between CrI₃ and Sc₂CO₂ layers. In Figure 2c, we plot the variation of charge densities of the heterostructures under opposite polarizations, in which the electron distribution of the carbon-down configuration is subtracted from that of the carbon-up configuration. In Figure 2c, despite complicated variations of the charge density in the Sc₂CO₂ layer due to the change of atomic positions related with ferroelectricity, we can see that there are extra electrons in the bilayer CrI₃ part of the carbon-up configuration, compared with that of the carbon-down configuration. According to the Bader's charge

analysis, there are around $0.1 e$ transferred from Sc_2CO_2 to CrI_3 in the carbon-up configuration, resulting in electron doping in CrI_3 . On the other hand, within the error bar of DFT calculations, we do not observe any significant charge transfer from Sc_2CO_2 to CrI_3 in the carbon-down configuration.

To further connect this charge transfer with the change of magnetism, we have checked the doping effect on free-standing bilayer CrI_3 . As shown in Figure 2d, the HT-phase bilayer CrI_3 experiences a phase transition from the interlayer AFM to FM phases under electron doping but not hole doping, and the critical electron doping density is less than $0.01 e$ per unit cell. In fact, such an electron-doping induced magnetic phase transition was observed in recent experiments of bilayer CrI_3 .^{41,42} Therefore, we conclude that the out-of-plane polarization of the Sc_2CO_2 layer dramatically changes the band alignment in the $\text{CrI}_3/\text{Sc}_2\text{CO}_2$ heterostructure, and the charge-transfer induced electron doping drives the magnetic phase transition of bilayer HT-phase CrI_3 .

The energy difference between energy gaps of the FM and AFM orderings may be the reason for the electron-doping induced magnetic crossover. According to our calculations, the energy gap of FM 2L- CrI_3 is about 70-meV smaller than that of AFM 2L- CrI_3 , which agrees with a previous calculation.⁵³ As a result, doped electrons will acquire less energy in the FM state than that in the AFM state. Given the small energy difference between the interlayer FM and AFM orderings (~ 0.37 meV), for a reduction of 70 meV of band gap, a doping density of $0.01 e/\text{unit-cell}$ can provide about 0.7 meV

energy gain of the AFM state than that of the FM state, making it possible to explain the energetic preference of the FM ground state. However, we have also noticed other mechanisms that can be applied to answering this question, such as the enhanced FM coupling mediated by interlayer electron hopping in itinerant electron systems.⁶²

In our studied heterostructures, because of the broken symmetry and existence of polarization field, the doped charge is mainly accumulated at the bottom layer of CrI₃. On the other hand, in our calculations to explain doping effects in free-standing 2L-CrI₃ structures, the doped charge is evenly distributed to both bottom and top layers due to the preservation of symmetry. In this sense, these two simulations are not perfectly consistent with each other. However, we believe that this may quantitatively affect our result but not fundamentally change the explanation and conclusion because the mechanism of the switch of magnetic ordering is from the band gap variation or itinerant electrons. Particularly, DFT may overestimate the inhomogeneous charge density under polarization field because it is known for not accurately capturing the screening effect. This is also evidenced by recent experiments, in which they gated and doped bilayer CrI₃ simultaneously.^{41,42} In those experiments, doped charge is biased by the gating field but accumulated slightly difference between the top and bottom layers. More future works are valuable to quantitatively investigate the inhomogeneous charge distribution in these heterostructures.

However, DFT calculations are known for underestimating the band gap of semiconductors and insulators. Therefore, the above bandgap closing may be an artificial result of DFT calculations. To answer this concern, we have employed the Heyd–Scuseria–Ernzerhof (HSE) hybrid functional⁶³ to check the band alignment in the CrI₃/Sc₂CO₂ heterostructure. Because of the large number (284) of electrons in one unit cell of the 2L-CrI₃/Sc₂CO₂ heterostructure, it is formidable to perform brute-force HSE calculations with spin-orbit coupling (SOC) included. In the following, we will do two approximations to obtain the band alignments.

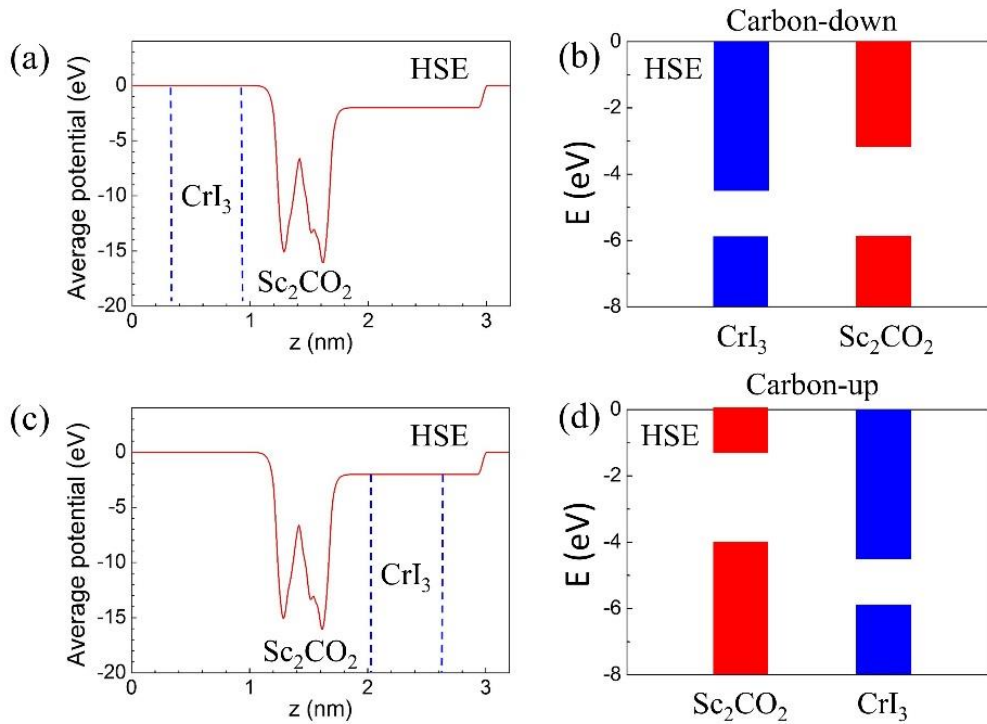


Figure 3. (a) Work function of Sc₂CO₂ calculated by HSE. (b) The band alignment of 2L-CrI₃/Sc₂CO₂ for the carbon-down configuration, in which CrI₃ is placed on the left side of Sc₂CO₂ as denoted by the two dashed lines in (a). (c) and (d) are similar to (a) and (b), but corresponding to the carbon-up configuration.

First, we perform the HSE calculations to obtain the work functions of isolated monolayer Sc_2CO_2 and 2L CrI_3 , respectively. As shown in Figure 3a, the vacuums at the two sides of the Sc_2CO_2 layer have different potentials due to its spontaneous out-of-plane electric polarization. This potential difference is about 2.0 eV, which imply a very strong built-in electric field. As shown in Figure 3a, the CrI_3 bilayer will feel two different potentials depending on the polarization direction, inducing two types of the energy alignment for CrI_3 and Sc_2CO_2 heterostructures. By comparing these absolute band energies, we obtain a type-II band alignment in the carbon-down configuration and a type III band alignment in the carbon-up configuration in the 2L- $\text{CrI}_3/\text{Sc}_2\text{CO}_2$ heterostructures, as shown in Figures 3b and 3d, respectively. This agrees with the bandgap closing and charge transfer results for the carbon-up configuration in DFT calculations.

The above work-function calculations ignore the interlayer interactions, which may introduce error bars. Therefore, we try the second approach, in which we directly calculate the density of states (DOS) of the heterostructure but with one layer of CrI_3 and one layer of Sc_2CO_2 heterostructure by HSE. As shown in **Figures 4a** and 4b, the band structure and work functions of monolayer and bilayer CrI_3 are similar because the localized d orbitals around band edges are not very sensitive to quantum confinement. Therefore, we can expect that the band alignment of the heterostructure made by monolayer CrI_3 and Sc_2CO_2 is similar to that made by bilayer CrI_3 and Sc_2CO_2 . As shown in Figures 4c and 4d, we find that it is a type II band alignment for the carbon-

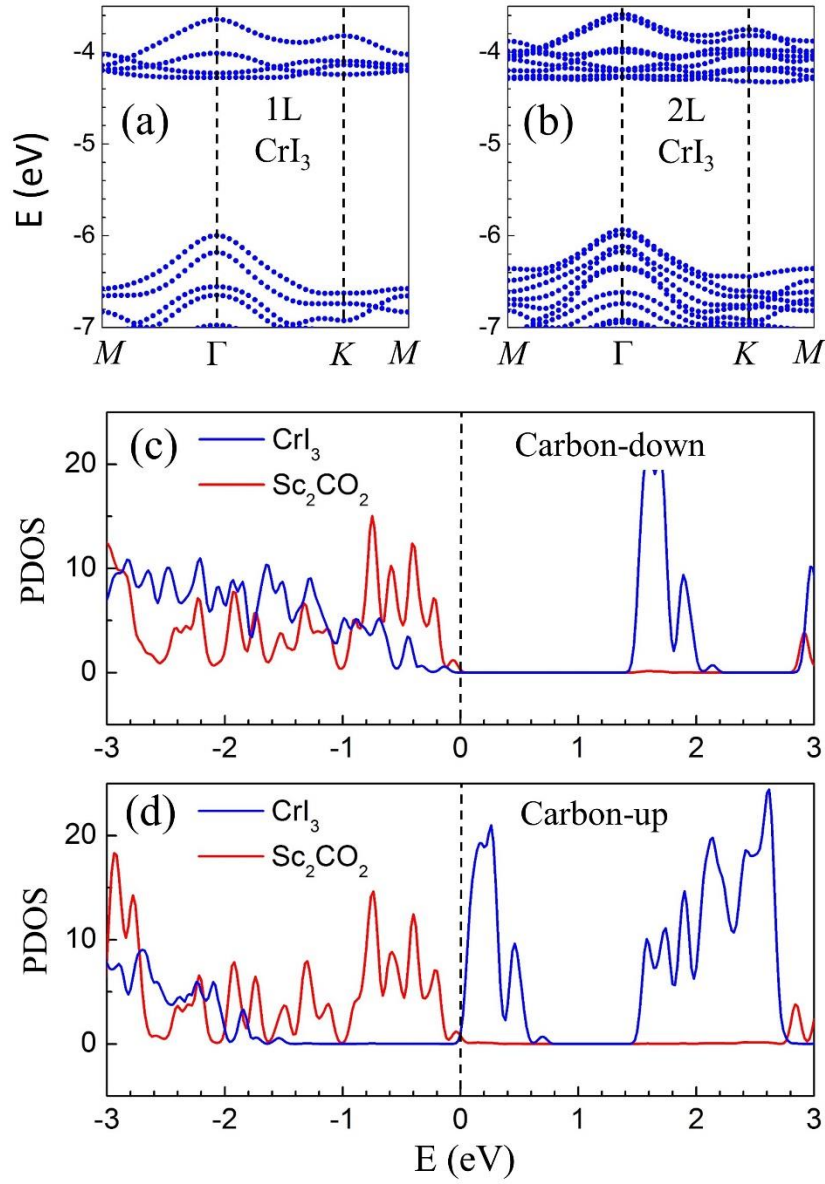


Figure 4. Band structures of (a) 1L-CrI₃ and (b) 2L-CrI₃ calculated by HSE. The HSE calculated PDOS of 1L-CrI₃/Sc₂CO₂ heterostructures with (c) carbon-down, and (d) carbon-up configurations. The blue and red curves are PDOS from CrI₃ and Sc₂CO₂, respectively.

down configuration and a type-III band alignment for the carbon-up configuration.

Therefore, these HSE calculations convince our previous charge-transfer conclusions

that the carbon-up configuration of $\text{CrI}_3/\text{Sc}_2\text{CO}_2$ is a type III metal state, which implies that the interlayer magnetic coupling of bilayer CrI_3 can also be changed from AFM to FM states when Sc_2CO_2 is changed from the carbon-down configuration to the carbon-up configuration.

Table 1. Energy difference between AFM and FM interlayer couplings of bilayer CrI_3 in the 2L- $\text{CrI}_3/\text{Sc}_2\text{CO}_2$ heterostructure calculated by different values of U and J .

$E_{\text{AFM}} - E_{\text{FM}}$ (meV/unit-cell)	$U = 3.9$ eV $J = 1.1$ eV	$U = 3.9$ eV $J = 0.0$ eV	$U = 2.9$ eV $J = 0.7$ eV	$U = 3.0$ eV $J = 0.0$ eV	$U = 3.9$ eV, $J = 1.1$ eV (fully relaxed)
Carbon-down	-0.37	-0.23	-0.27	-0.39	-0.32
Carbon-up	1.41	3.41	2.27	2.6	1.60

It is known challenging for DFT simulations to describe the correlated effects in magnetic materials. Similar to most previous works in this field, we have employed the DFT+ U approach to capture the localized d orbitals. In this work, we choose the Liechtenstein scheme with $U = 3.9$ eV and $J = 1.1$ eV, which are calculated by the linear response method and have been successfully applied to explaining the observed AFM and FM interlayer magnetic orders of HT and LT phases of few-layer CrI_3 .⁵³ On the other hand, to further confirm that our above conclusions are robust against the choices of U and J parameters, we have done the calculations with different values of U and J within a reasonable range, as used in previous calculations.^{54–56} As summarized in **Table 1**, all these choices give the same conclusion that the AFM interlayer order is the

ground state for the carbon-down configuration of Sc_2CO_2 , and the FM interlayer order is the ground state of the carbon-up configuration of Sc_2CO_2 .

It is interesting to check whether the magnetic easy axis of 2L- CrI_3 can be turned by ferroelectric states of Sc_2CO_2 since the switch of magnetic easy axis was predicted in $\text{Cr}_2\text{Ge}_2\text{Te}_3$ and charge doped CrSBr .^{49,64} We have calculated the magnetic anisotropy energy (MAE), defined by the energy difference between magnetic states with out-of-plane and in-plane spins of 2L- CrI_3 under two ferroelectric states of Sc_2CO_2 in the heterostructure. The calculated results are shown in Table 2. We can see that MAE is different between the Carbon-up and Carbon-down ferroelectric states, although these energy differences also depend on the values of U and J in first-principles calculations. Generally, the carbon-up polarization introduces doped carriers to bilayer CrI_3 . As a result, for most choices of U and J , the MAE energy under the carbon-up configuration has a smaller MAE. This agrees with previous doping calculations of monolayer CrI_3 .⁶⁵

Table 2. Energy difference between magnetic states with out-of-plane spins and in-plane spins of bilayer CrI_3 in the 2L- $\text{CrI}_3/\text{Sc}_2\text{CO}_2$ heterostructure calculated by different values of U and J .

<i>MAE</i> (meV/unit-cell)	U = 3.9 eV J = 1.1 eV	U = 3.9 eV J = 0.0 eV	U = 2.9 eV J = 0.7 eV	U = 3.0 eV J = 0.0 eV	U = 3.9 eV, J = 1.1eV (fully relaxed)
Carbon-down	-1.13	-2.69	-1.62	-2.62	-1.18
Carbon-up	-0.32	-3.17	-1.2	-2.5	-1.21

At last, we will estimate the working temperature for 2L-CrI₃/Sc₂CO₂ heterostructure. For the ferroelectric Curie temperature, the ferroelectric transition barrier was found to be 0.52 eV per formula unit for Sc₂CO₂.¹⁹ Thus, the ferroelectric Curie temperature can be up to room temperature. In this sense, the working temperature for the 2L-CrI₃/Sc₂CO₂ heterostructure is determined by the Néel temperature of 2L-CrI₃. In our structure, we do not observe significant changes of exchange couplings of CrI₃ in this heterostructure. Therefore, we estimate that the Néel temperature is similar to the result of free-standing cases, which is about 41 K observed by experiments.²⁴ This indicates that the upper limit of the working temperature of multiferroics is around 41 K.

3. CONCLUSIONS

We propose artificial multiferroics in a vdW heterostructure formed by bilayer CrI₃ and monolayer Sc₂CO₂. Particularly, an enhanced magnetoelectric effect is predicted: the switch of electronic polarization in the FE Sc₂CO₂ layer can switch the interlayer magnetic coupling of bilayer CrI₃, switching the interlayer FM/AFM magnetic ordering of bilayer CrI₃. We further show that the strong build-in electric field in the Sc₂CO₂ layer alters the energy band alignment of the heterostructure between type II and type III. In the type III band alignment, the charge transfer between CrI₃ and Sc₂CO₂ converts the interlayer magnetic coupling from AFM to FM. Our finding provides a general method to construct 2D artificial-multiferroic devices by stacking of 2D ferroic vdW materials, shedding light on realizing multifunctional nanoelectronic devices.

4. COMPUTATIONAL METHOD

Calculations are performed by using first-principles density functional theory (DFT) as implemented in *Vienna Ab initio Simulation Package* (VASP),^{66,67} with the dispersion-corrected PBEsol⁶⁸ and HSE⁶³ functional. The first Brillouin zone is sampled with the $9\times 9\times 1$ and $6\times 6\times 1$ k-point meshes for DFT and HSE calculations, respectively. A plane-wave basis set with a kinetic energy cutoff of 450 eV is adopted throughout these calculations. A vacuum distance larger than 15 Å is set between adjacent slabs to avoid spurious interactions. The main data are calculated by the GGA+U functional based on the Liechtenstein scheme⁶⁹ with $U = 3.9$ eV and $J = 1.1$ eV. Other values of U and J have also been tested and give qualitatively similar results. Dipole corrections and SOC are included in all calculations. The differential charge distributions are visualized by the VESTA software.⁷⁰

For structure relaxations, all atoms are relaxed until the residual force per atom is less than 0.005 eV/Å. Because of the lattice mismatch, we fix the experimental in-plane lattice constant of CrI₃ and relax all other degree of freedom of the heterostructure. Meanwhile, we have calculated the fully relaxed structure and do not find any qualitatively change of our results. (see the last column of Table 1) Moreover, as shown in Figure 1a, the lowest-energy stacking configuration of bilayer CrI₃ and Sc₂CO₂ is that the middle-layer Cr atoms are on top of O and C atoms of the bottom Sc₂CO₂ layer.

Other interlayer configurations have been checked, and they do not qualitatively change the results.

AUTHOR INFORMATION

Corresponding Authors

*E-mail: liwang@ncu.edu.cn (L.W.)

*E-mail: lyang@physics.wustl.edu (L.Y.)

Notes

The authors declare no competing financial interest.

ACKNOWLEDGEMENTS

Y.L. is supported by the Natural Science Foundation of China (Grant No. 11504158) and China Scholarship Council. L.Y., R.F., X.L., and L.Z. are supported by the National Science Foundation (NSF) CAREER Grant No. DMR-1455346 and the Air Force Office of Scientific Research (AFOSR) grant No. FA9550-17-1-0304. The computational resources have been provided by the Stampede of Teragrid at the Texas Advanced Computing Center (TACC) through XSEDE.

References

- (1) Kimura, T.; Goto, T.; Shintani, H.; Ishizaka, K.; Arima, T.; Tokura, Y. Magnetic Control of Ferroelectric Polarization. *Nature* **2003**, *426* (6962), 55–58. <https://doi.org/10.1038/nature02018>.
- (2) Chu, Y. H.; Martin, L. W.; Holcomb, M. B.; Gajek, M.; Han, S. J.; He, Q.; Balke, N.; Yang, C. H.; Lee, D.; Hu, W.; Zhan, Q.; Yang, P.-L.; Fraile-Rodriguez, A.; Scholl, A.; Wang, S. X.; Ramesh, R. Electric-Field Control of Local Ferromagnetism Using a Magnetoelectric Multiferroic. *Nat. Mater.* **2008**, *7* (6), 478–482. <https://doi.org/10.1038/nmat2184>.
- (3) Wang, K. F.; Liu, J. M.; Ren, Z. F. Multiferroicity: The Coupling between Magnetic and Polarization Orders. *Adv. Phys.* **2009**, *58* (4), 321–448. <https://doi.org/10.1080/00018730902920554>.
- (4) Hill, N. A. Why Are There so Few Magnetic Ferroelectrics? *J. Phys. Chem. B* **2000**, *104* (29), 6694–6709. <https://doi.org/10.1021/jp000114x>.
- (5) Wu, M.; Zeng, X. C. Intrinsic Ferroelasticity and/or Multiferroicity in Two-Dimensional Phosphorene and Phosphorene Analogues. *Nano Lett.* **2016**, *16* (5), 3236–3241. <https://doi.org/10.1021/acs.nanolett.6b00726>.
- (6) Hanakata, P. Z.; Carvalho, A.; Campbell, D. K.; Park, H. S. Polarization and Valley Switching in Monolayer Group-IV Monochalcogenides. *Phys. Rev. B* **2016**, *94* (3), 035304. <https://doi.org/10.1103/PhysRevB.94.035304>.
- (7) Fei, R.; Kang, W.; Yang, L. Ferroelectricity and Phase Transitions in Monolayer Group-IV Monochalcogenides. *Phys. Rev. Lett.* **2016**, *117* (9),

097601. <https://doi.org/10.1103/PhysRevLett.117.097601>.
- (8) Mehboudi, M.; Fregoso, B. M.; Yang, Y.; Zhu, W.; van der Zande, A.; Ferrer, J.; Bellaiche, L.; Kumar, P.; Barraza-Lopez, S. Structural Phase Transition and Material Properties of Few-Layer Monochalcogenides. *Phys. Rev. Lett.* **2016**, *117* (24), 246802. <https://doi.org/10.1103/PhysRevLett.117.246802>.
- (9) Chang, K.; Liu, J.; Lin, H.; Wang, N.; Zhao, K.; Zhang, A.; Jin, F.; Zhong, Y.; Hu, X.; Duan, W.; Zhang, Q.; Fu, L.; Xue, Q.-K.; Chen, X.; Ji, S.-H. Discovery of Robust In-Plane Ferroelectricity in Atomic-Thick SnTe. *Science* **2016**, *353* (6296), 274–278. <https://doi.org/10.1126/science.aad8609>.
- (10) Xiao, C.; Wang, F.; Yang, S. A.; Lu, Y.; Feng, Y.; Zhang, S. Elemental Ferroelectricity and Antiferroelectricity in Group-V Monolayer. *Adv. Funct. Mater.* **2018**, *28* (17), 1707383. <https://doi.org/10.1002/adfm.201707383>.
- (11) Ding, W.; Zhu, J.; Wang, Z.; Gao, Y.; Xiao, D.; Gu, Y.; Zhang, Z.; Zhu, W. Prediction of Intrinsic Two-Dimensional Ferroelectrics in In₂Se₃ and Other III₂-VI₃ van Der Waals Materials. *Nat. Commun.* **2017**, *8* (1), 14956. <https://doi.org/10.1038/ncomms14956>.
- (12) Zhou, Y.; Wu, D.; Zhu, Y.; Cho, Y.; He, Q.; Yang, X.; Herrera, K.; Chu, Z.; Han, Y.; Downer, M. C.; Peng, H.; Lai, K. Out-of-Plane Piezoelectricity and Ferroelectricity in Layered α -In₂Se₃ Nanoflakes. *Nano Lett.* **2017**, *17* (9), 5508–5513. <https://doi.org/10.1021/acs.nanolett.7b02198>.
- (13) Zheng, C.; Yu, L.; Zhu, L.; Collins, J. L.; Kim, D.; Lou, Y.; Xu, C.; Li, M.; Wei, Z.; Zhang, Y.; Edmonds, M. T.; Li, S.; Seidel, J.; Zhu, Y.; Liu, J. Z.;

- Tang, W.-X.; Fuhrer, M. S. Room Temperature In-Plane Ferroelectricity in van Der Waals In₂Se₃. *Sci. Adv.* **2018**, *4* (7), eaar7720.
<https://doi.org/10.1126/sciadv.aar7720>.
- (14) Cui, C.; Hu, W.-J.; Yan, X.; Addiego, C.; Gao, W.; Wang, Y.; Wang, Z.; Li, L.; Cheng, Y.; Li, P.; Zhang, X.; Alshareef, H. N.; Wu, T.; Zhu, W.; Pan, X.; Li, L.-J. Intercorrelated In-Plane and Out-of-Plane Ferroelectricity in Ultrathin Two-Dimensional Layered Semiconductor In₂Se₃. *Nano Lett.* **2018**, *18* (2), 1253–1258. <https://doi.org/10.1021/acs.nanolett.7b04852>.
- (15) Xue, F.; Hu, W.; Lee, K.; Lu, L.; Zhang, J.; Tang, H.; Han, A.; Hsu, W.; Tu, S.; Chang, W.; Lien, C.-H.; He, J.-H.; Zhang, Z.; Li, L.-J.; Zhang, X. Room - Temperature Ferroelectricity in Hexagonally Layered A - In₂Se₃ Nanoflakes down to the Monolayer Limit. *Adv. Funct. Mater.* **2018**, *28* (50), 1803738.
<https://doi.org/10.1002/adfm.201803738>.
- (16) Liu, F.; You, L.; Seyler, K. L.; Li, X.; Yu, P.; Lin, J.; Wang, X.; Zhou, J.; Wang, H.; He, H.; Pantelides, T.; Zhou, W.; Sharma, P.; Xu, X.; Ajayan, P. M.; Wang, J.; Liu, Z. Room-Temperature Ferroelectricity in CuInP₂S₆ Ultrathin Flakes. *Nat. Commun.* **2016**, *7* (1), 12357.
<https://doi.org/10.1038/ncomms12357>.
- (17) Xu, B.; Xiang, H.; Xia, Y.; Jiang, K.; Wan, X.; He, J.; Yin, J.; Liu, Z. Monolayer AgBiP₂Se₆ : An Atomically Thin Ferroelectric Semiconductor with out-Plane Polarization. *Nanoscale* **2017**, *9* (24), 8427–8434.
<https://doi.org/10.1039/C7NR02461D>.

- (18) Song, W.; Fei, R.; Yang, L. Off-Plane Polarization Ordering in Metal Chalcogen Diphosphates from Bulk to Monolayer. *Phys. Rev. B* **2017**, *96* (23), 235420. <https://doi.org/10.1103/PhysRevB.96.235420>.
- (19) Lai, Y.; Song, Z.; Wan, Y.; Xue, M.; Wang, C.; Ye, Y.; Dai, L.; Zhang, Z.; Yang, W.; Du, H.; Yang, J. Two-Dimensional Ferromagnetism and Driven Ferroelectricity in van Der Waals CuCrP₂S₆. *Nanoscale* **2019**, *11* (12), 5163–5170. <https://doi.org/10.1039/C9NR00738E>.
- (20) Chandrasekaran, A.; Mishra, A.; Singh, A. K. Ferroelectricity, Antiferroelectricity, and Ultrathin 2D Electron/Hole Gas in Multifunctional Monolayer MXene. *Nano Lett.* **2017**, *17* (5), 3290–3296. <https://doi.org/10.1021/acs.nanolett.7b01035>.
- (21) Wu, M.; Jena, P. The Rise of Two-Dimensional van Der Waals Ferroelectrics. *Wiley Interdiscip. Rev. Comput. Mol. Sci.* **2018**, *8* (5), e1365. <https://doi.org/10.1002/wcms.1365>.
- (22) Cui, C.; Xue, F.; Hu, W.-J.; Li, L.-J. Two-Dimensional Materials with Piezoelectric and Ferroelectric Functionalities. *npj 2D Mater. Appl.* **2018**, *2* (1), 18. <https://doi.org/10.1038/s41699-018-0063-5>.
- (23) Hu, T.; Kan, E. Progress and Prospects in Low-Dimensional Multiferroic Materials. *Wiley Interdiscip. Rev. Comput. Mol. Sci.* **2019**, *9* (5), e1409. <https://doi.org/10.1002/wcms.1409>.
- (24) Gong, C.; Li, L.; Li, Z.; Ji, H.; Stern, A.; Xia, Y.; Cao, T.; Bao, W.; Wang, C.; Wang, Y.; Qiu, Z. Q.; Cava, R. J.; Louie, S. G.; Xia, J.; Zhang, X. Discovery of

- Intrinsic Ferromagnetism in Two-Dimensional van Der Waals Crystals. *Nature* **2017**, *546* (7657), 265–269. <https://doi.org/10.1038/nature22060>.
- (25) Huang, B.; Clark, G.; Navarro-Moratalla, E.; Klein, D. R.; Cheng, R.; Seyler, K. L.; Zhong, Di.; Schmidgall, E.; McGuire, M. A.; Cobden, D. H.; Yao, W.; Xiao, D.; Jarillo-Herrero, P.; Xu, X. Layer-Dependent Ferromagnetism in a van Der Waals Crystal down to the Monolayer Limit. *Nature* **2017**, *546* (7657), 270–273. <https://doi.org/10.1038/nature22391>.
- (26) Fei, Z.; Huang, B.; Malinowski, P.; Wang, W.; Song, T.; Sanchez, J.; Yao, W.; Xiao, D.; Zhu, X.; May, A. F.; Wu, W.; Cobden, D. H.; Chu, J.-H.; Xu, X. Two-Dimensional Itinerant Ferromagnetism in Atomically Thin Fe₃GeTe₂. *Nat. Mater.* **2018**, *17* (9), 778–782. <https://doi.org/10.1038/s41563-018-0149-7>.
- (27) Deng, Y.; Yu, Y.; Song, Y.; Zhang, J.; Wang, N. Z.; Sun, Z.; Yi, Y.; Wu, Y. Z.; Wu, S.; Zhu, J.; Wang, J.; Chen, X. H.; Zhang, Y. Gate-Tunable Room-Temperature Ferromagnetism in Two-Dimensional Fe₃GeTe₂. *Nature* **2018**, *563* (7729), 94–99. <https://doi.org/10.1038/s41586-018-0626-9>.
- (28) McGuire, M. A.; Dixit, H.; Cooper, V. R.; Sales, B. C. Coupling of Crystal Structure and Magnetism in the Layered, Ferromagnetic Insulator CrI₃. *Chem. Mater.* **2015**, *27* (2), 612–620. <https://doi.org/10.1021/cm504242t>.
- (29) Jiang, P.; Li, L.; Liao, Z.; Zhao, Y. X.; Zhong, Z. Spin Direction-Controlled Electronic Band Structure in Two-Dimensional Ferromagnetic CrI₃. *Nano Lett.* **2018**, *18* (6), 3844–3849. <https://doi.org/10.1021/acs.nanolett.8b01125>.
- (30) Song, T.; Tu, M. W.-Y.; Carnahan, C.; Cai, X.; Taniguchi, T.; Watanabe, K.;

- McGuire, M. A.; Cobden, D. H.; Xiao, D.; Yao, W.; Xu, X. Voltage Control of a van Der Waals Spin-Filter Magnetic Tunnel Junction. *Nano Lett.* **2019**, *19* (2), 915–920. <https://doi.org/10.1021/acs.nanolett.8b04160>.
- (31) Seyler, K. L.; Zhong, D.; Klein, D. R.; Gao, S.; Zhang, X.; Huang, B.; Navarro-Moratalla, E.; Yang, L.; Cobden, D. H.; McGuire, M. A.; Yao, W.; Xiao, D.; Jarillo-Herrero, P.; Xu, X. Ligand-Field Helical Luminescence in a 2D Ferromagnetic Insulator. *Nat. Phys.* **2018**, *14* (3), 277–281. <https://doi.org/10.1038/s41567-017-0006-7>.
- (32) Wu, M.; Li, Z.; Cao, T.; Louie, S. G. Physical Origin of Giant Excitonic and Magneto-Optical Responses in Two-Dimensional Ferromagnetic Insulators. *Nat. Commun.* **2019**, *10* (1), 2371. <https://doi.org/10.1038/s41467-019-10325-7>.
- (33) Klein, D. R.; MacNeill, D.; Song, Q.; Larson, D. T.; Fang, S.; Xu, M.; Ribeiro, R. A.; Canfield, P. C.; Kaxiras, E.; Comin, R.; Jarillo-Herrero, P. Enhancement of Interlayer Exchange in an Ultrathin Two-Dimensional Magnet. *Nat. Phys.* **2019**, 1–6. <https://doi.org/10.1038/s41567-019-0651-0>.
- (34) Kim, H. H.; Yang, B.; Li, S.; Jiang, S.; Jin, C.; Tao, Z.; Nichols, G.; Sfigakis, F.; Zhong, S.; Li, C.; Tian, S.; Cory, D. G.; Miao, G.-X.; Shan, J.; Mak, K. F.; Lei, H.; Sun, K.; Zhao, L.; Tsien, A. W. Evolution of Interlayer and Intralayer Magnetism in Three Atomically Thin Chromium Trihalides. *Proc. Natl. Acad. Sci.* **2019**, *116* (23), 11131–11136. <https://doi.org/10.1073/pnas.1902100116>.
- (35) Gong, C.; Zhang, X. Two-Dimensional Magnetic Crystals and Emergent

- Heterostructure Devices. *Science* **2019**, *363* (6428), eaav4450.
<https://doi.org/10.1126/science.aav4450>.
- (36) Thiel, L.; Wang, Z.; Tschudin, M. A.; Rohner, D.; Gutiérrez-Lezama, I.; Ubrig, N.; Gibertini, M.; Giannini, E.; Morpurgo, A. F.; Maletinsky, P. Probing Magnetism in 2D Materials at the Nanoscale with Single-Spin Microscopy. *Science* **2019**, *364* (6444), 973–976. <https://doi.org/10.1126/science.aav6926>.
- (37) Gibertini, M.; Koperski, M.; Morpurgo, A. F.; Novoselov, K. S. Magnetic 2D Materials and Heterostructures. *Nat. Nanotechnol.* **2019**, *14* (5), 408–419.
<https://doi.org/10.1038/s41565-019-0438-6>.
- (38) Zhao, Y.; Lin, L.; Zhou, Q.; Li, Y.; Yuan, S.; Chen, Q.; Dong, S.; Wang, J. Surface Vacancy-Induced Switchable Electric Polarization and Enhanced Ferromagnetism in Monolayer Metal Trihalides. *Nano Lett.* **2018**, *18* (5), 2943–2949. <https://doi.org/10.1021/acs.nanolett.8b00314>.
- (39) Burch, K. S.; Mandrus, D.; Park, J.-G. Magnetism in Two-Dimensional van Der Waals Materials. *Nature* **2018**, *563* (7729), 47–52.
<https://doi.org/10.1038/s41586-018-0631-z>.
- (40) Jiang, S.; Shan, J.; Mak, K. F. Electric-Field Switching of Two-Dimensional van Der Waals Magnets. *Nat. Mater.* **2018**, *17* (5), 406–410.
<https://doi.org/10.1038/s41563-018-0040-6>.
- (41) Wang, Z.; Zhang, T.; Ding, M.; Dong, B.; Li, Y.; Chen, M.; Li, X.; Huang, J.; Wang, H.; Zhao, X.; Li, Y.; Li, D.; Jia, C.; Sun, L.; Guo, H.; Ye, Y.; Sun, D.; Chen, Y.; Yang, T.; Zhang, J.; One, S.; Han, Z.; Zhang, Z. Electric-Field

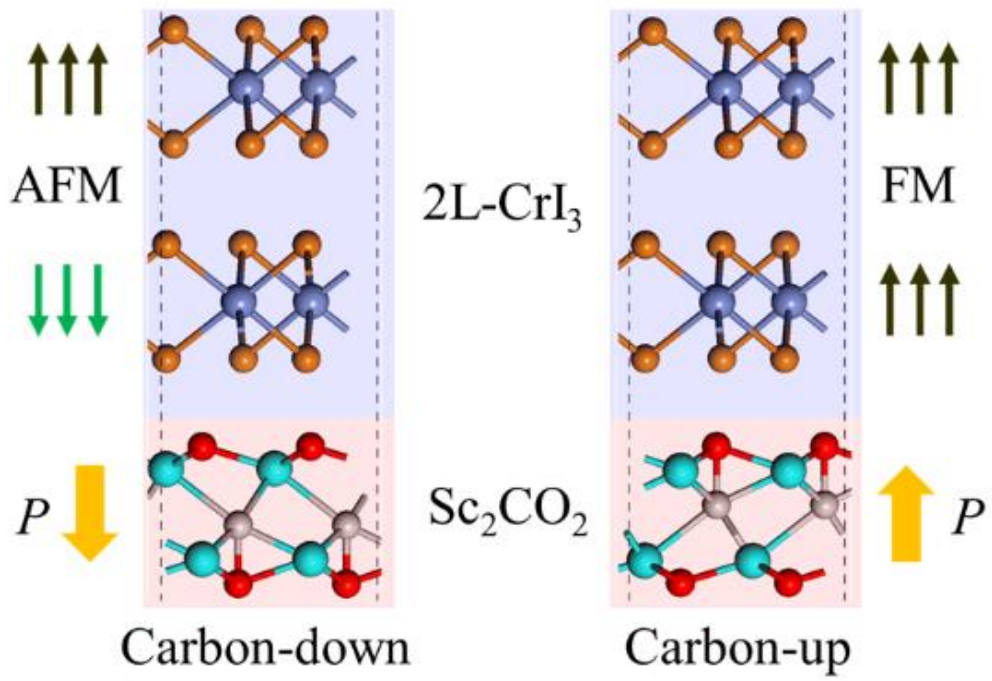
- Control of Magnetism in a Few-Layered van Der Waals Ferromagnetic Semiconductor. *Nat. Nanotechnol.* **2018**, *13* (7), 554–559.
<https://doi.org/10.1038/s41565-018-0186-z>.
- (42) Huang, B.; Clark, G.; Klein, D. R.; MacNeill, D.; Navarro-Moratalla, E.; Seyler, K. L.; Wilson, N.; McGuire, M. A.; Cobden, D. H.; Xiao, D.; Yao, W.; Jarillo-Herrero, P.; Xu, X. Electrical Control of 2D Magnetism in Bilayer CrI₃. *Nat. Nanotechnol.* **2018**, *13* (7), 544–548. <https://doi.org/10.1038/s41565-018-0121-3>.
- (43) Jiang, S.; Li, L.; Wang, Z.; Mak, K. F.; Shan, J. Controlling Magnetism in 2D CrI₃ by Electrostatic Doping. *Nat. Nanotechnol.* **2018**, *13* (7), 549–553.
<https://doi.org/10.1038/s41565-018-0135-x>.
- (44) Klein, D. R.; MacNeill, D.; Lado, J. L.; Soriano, D.; Navarro-Moratalla, E.; Watanabe, K.; Taniguchi, T.; Manni, S.; Canfield, P.; Fernández-Rossier, J.; Jarillo-Herrero, P. Probing Magnetism in 2D van Der Waals Crystalline Insulators via Electron Tunneling. *Science* **2018**, *360* (6394), 1218–1222.
<https://doi.org/10.1126/science.aar3617>.
- (45) Song, T.; Cai, X.; Tu, M. W.-Y.; Zhang, X.; Huang, B.; Wilson, N. P.; Seyler, K. L.; Zhu, L.; Taniguchi, T.; Watanabe, K.; McGuire, M. A.; Cobden, D. H.; Xiao, D.; Yao, W.; Xu, X. Giant Tunneling Magnetoresistance in Spin-Filter van Der Waals Heterostructures. *Science* **2018**, *360* (6394), 1214–1218.
<https://doi.org/10.1126/science.aar4851>.
- (46) Wang, H.; Qian, X. Two-Dimensional Multiferroics in Monolayer Group IV

- Monochalcogenides. *2D Mater.* **2017**, *4* (1), 015042.
<https://doi.org/10.1088/2053-1583/4/1/015042>.
- (47) Qi, J.; Wang, H.; Chen, X.; Qian, X. Two-Dimensional Multiferroic Semiconductors with Coexisting Ferroelectricity and Ferromagnetism. *Appl. Phys. Lett.* **2018**, *113* (4), 043102. <https://doi.org/10.1063/1.5038037>.
- (48) Huang, C.; Du, Y.; Wu, H.; Xiang, H.; Deng, K.; Kan, E. Prediction of Intrinsic Ferromagnetic Ferroelectricity in a Transition-Metal Halide Monolayer. *Phys. Rev. Lett.* **2018**, *120* (14), 147601.
<https://doi.org/10.1103/PhysRevLett.120.147601>.
- (49) Gong, C.; Kim, E. M.; Wang, Y.; Lee, G.; Zhang, X. Multiferroicity in Atomic van Der Waals Heterostructures. *Nat. Commun.* **2019**, *10* (1), 2657.
<https://doi.org/10.1038/s41467-019-10693-0>.
- (50) Hou, Y.; Kim, J.; Wu, R. Magnetizing Topological Surface States of Bi₂Se₃ with a CrI₃ Monolayer. *Sci. Adv.* **2019**, *5* (5), eaaw1874.
<https://doi.org/10.1126/sciadv.aaw1874>.
- (51) Zollner, K.; Faria Junior, P. E.; Fabian, J. Proximity exchange effects in MoSe₂ and WSe₂ heterostructures with CrI₃: Twist angle, layer, and gate dependence. *Phys. Rev. B* **2019**, *100* (8), 085128.
<https://doi.org/10.1103/PhysRevB.100.085128>.
- (52) Lado, J. L.; Fernández-Rossier, J. On the Origin of Magnetic Anisotropy in Two Dimensional CrI₃. *2D Mater.* **2017**, *4* (3), 035002.
<https://doi.org/10.1088/2053-1583/aa75ed>.

- (53) Jiang, P.; Wang, C.; Chen, D.; Zhong, Z.; Yuan, Z.; Lu, Z.-Y.; Ji, W. Stacking Tunable Interlayer Magnetism in Bilayer CrI₃. *Phys. Rev. B* **2019**, *99* (14), 144401. <https://doi.org/10.1103/PhysRevB.99.144401>.
- (54) Sivadas, N.; Okamoto, S.; Xu, X.; Fennie, C. J.; Xiao, D. Stacking-Dependent Magnetism in Bilayer CrI₃. *Nano Lett.* **2018**, *18* (12), 7658–7664. <https://doi.org/10.1021/acs.nanolett.8b03321>.
- (55) Jang, S. W.; Jeong, M. Y.; Yoon, H.; Ryee, S.; Han, M. J. Microscopic Understanding of Magnetic Interactions in Bilayer CrI₃. *Phys. Rev. Mater.* **2019**, *3* (3), 031001. <https://doi.org/10.1103/PhysRevMaterials.3.031001>.
- (56) Soriano, D.; Cardoso, C.; Fernández-Rossier, J. Interplay between Interlayer Exchange and Stacking in CrI₃ Bilayers. *Solid State Commun.* **2019**, *299*, 113662. <https://doi.org/10.1016/j.ssc.2019.113662>.
- (57) Wang, Z.; Gutiérrez-Lezama, I.; Ubrig, N.; Kroner, M.; Gibertini, M.; Taniguchi, T.; Watanabe, K.; Imamoğlu, A.; Giannini, E.; Morpurgo, A. F. Very Large Tunneling Magnetoresistance in Layered Magnetic Semiconductor CrI₃. *Nat. Commun.* **2018**, *9* (1), 2516. <https://doi.org/10.1038/s41467-018-04953-8>.
- (58) Kim, H. H.; Yang, B.; Patel, T.; Sfigakis, F.; Li, C.; Tian, S.; Lei, H.; Tsen, A. W. One Million Percent Tunnel Magnetoresistance in a Magnetic van Der Waals Heterostructure. *Nano Lett.* **2018**, *18* (8), 4885–4890. <https://doi.org/10.1021/acs.nanolett.8b01552>.
- (59) Song, T.; Fei, Z.; Yankowitz, M.; Lin, Z.; Jiang, Q.; Hwangbo, K.; Zhang, Q.;

- Sun, B.; Taniguchi, T.; Watanabe, K.; McGuire, M. A.; Graf, D.; Cao, T.; Chu, J.-H.; Cobden, D. H.; Dean, C. R.; Xiao, D.; Xu, X. Switching 2D Magnetic States via Pressure Tuning of Layer Stacking. *Nat. Mater.* **2019**, *18* (12), 1298–1302. <https://doi.org/10.1038/s41563-019-0505-2>.
- (60) Li, T.; Jiang, S.; Sivadas, N.; Wang, Z.; Xu, Y.; Weber, D.; Goldberger, J. E.; Watanabe, K.; Taniguchi, T.; Fennie, C. J.; Mak, K. F.; Shan, J. Pressure-Controlled Interlayer Magnetism in Atomically Thin CrI₃. *Nat. Mater.* **2019**, *18* (12), 1303–1308. <https://doi.org/10.1038/s41563-019-0506-1>.
- (61) Sun, Z.; Yi, Y.; Song, T.; Clark, G.; Huang, B.; Shan, Y.; Wu, S.; Huang, D.; Gao, C.; Chen, Z.; McGuire, M.; Cao, T.; Xiao, D.; Liu, W.-T.; Yao, W.; Xu, X.; Wu, S. Giant Nonreciprocal Second-Harmonic Generation from Antiferromagnetic Bilayer CrI₃. *Nature* **2019**, *572* (7770), 497–501. <https://doi.org/10.1038/s41586-019-1445-3>.
- (62) Sakai, S.; Arita, R.; Aoki, H. Itinerant Ferromagnetism in the Multiorbital Hubbard Model: A Dynamical Mean-Field Study. *Phys. Rev. Lett.* **2007**, *99* (21), 216402. <https://doi.org/10.1103/PhysRevLett.99.216402>.
- (63) Heyd, J.; Scuseria, G. E.; Ernzerhof, M. Hybrid Functionals Based on a Screened Coulomb Potential. *J. Chem. Phys.* **2003**, *118* (18), 8207–8215. <https://doi.org/10.1063/1.1564060>.
- (64) Qi, J.; Wang, H.; Qian, X. Electrically Tunable, High Curie Temperature 2D Ferromagnetism in Van Der Waals Layered Crystals. *arXiv:1811.02674*. <https://doi.org/arXiv:1811.02674>.

- (65) Zheng, F.; Zhao, J.; Liu, Z.; Li, M.; Zhou, M.; Zhang, S.; Zhang, P. Tunable Spin States in the Two-Dimensional Magnet CrI₃. *Nanoscale* **2018**, *10* (29), 14298–14303. <https://doi.org/10.1039/C8NR03230K>.
- (66) Kresse, G.; Furthmüller, J. Efficient Iterative Schemes for Ab Initio Total-Energy Calculations Using a Plane-Wave Basis Set. *Phys. Rev. B* **1996**, *54* (16), 11169–11186. <https://doi.org/10.1103/PhysRevB.54.11169>.
- (67) Kresse, G.; Joubert, D. From Ultrasoft Pseudopotentials to the Projector Augmented-Wave Method. *Phys. Rev. B* **1999**, *59* (3), 1758–1775. <https://doi.org/10.1103/PhysRevB.59.1758>.
- (68) Perdew, J. P.; Ruzsinszky, A.; Csonka, G. I.; Vydrov, O. A.; Scuseria, G. E.; Constantin, L. A.; Zhou, X.; Burke, K. Restoring the Density-Gradient Expansion for Exchange in Solids and Surfaces. *Phys. Rev. Lett.* **2008**, *100* (13), 136406. <https://doi.org/10.1103/PhysRevLett.100.136406>.
- (69) Liechtenstein, A. I.; Anisimov, V. I.; Zaanen, J. Density-Functional Theory and Strong Interactions: Orbital Ordering in Mott-Hubbard Insulators. *Phys. Rev. B* **1995**, *52* (8), R5467–R5470. <https://doi.org/10.1103/PhysRevB.52.R5467>.
- (70) Momma, K.; Izumi, F. VESTA 3 for Three-Dimensional Visualization of Crystal, Volumetric and Morphology Data. *J. Appl. Crystallogr.* **2011**, *44* (6), 1272–1276. <https://doi.org/10.1107/S0021889811038970>.



For Table of Contents Only